Effects of crystal defects and their interactions with impurities on electrical properties of multicrystalline Si

Supawan Joonwichien,[a] Satoru Matsushima, and Noritaka Usami
Institute for Materials Research, Tohoku University, 2-1-1 Katahira, Aoba-ku, Sendai 980-8577, Japan

(Received 18 December 2012; accepted 15 March 2013; published online 1 April 2013)

We investigated the effects of different crystal defects and their interactions with impurities on the electrical properties of multicrystalline Si (mc-Si) using samples with unique defect patterns and impurities. By using the floating cast method, a single grain boundary (GB), identified as a Σ27 boundary, was first formed with a high density of impurities from atmosphere, leading to an inefficient external gettering of impurities during phosphorus (P) diffusion. During crystal growth, the Σ27 GB splits into the Σ3 and Σ9 GBs with accompanying generation of dislocations and reduction in the density of impurities. The external gettering of impurities became efficient for removing impurities as evidenced by an increase in average minority carrier lifetime. At the final stage of crystal growth, the decrease in minority carrier lifetime was significant, which could not be improved by phosphorus diffusion because of the high densities of segregated impurities and crystal defects originating from the strong contact with the crucible. The increase in Σ number was found to result in more enhanced precipitation of impurities, which led to the poor gettering effect of P diffusion. These results further confirmed the importance of the reduction in the densities of impurities and dislocations for the quality and yield improvement of mc-Si ingots for solar cells.
 [http://dx.doi.org/10.1063/1.4798600]

I. INTRODUCTION

Crystal defects such as grain boundaries (GBs) and dislocations are among the major detrimental defects in multicrystalline Si (mc-Si), limiting the performance of solar cells. They contribute significantly to the recombination of excess charge carriers,[1–3] and the carrier lifetime or diffusion length generally decreases with increasing dislocation density.[4] Many attempts have been made to understand the effects of crystal defects and impurities on electrical properties that affect solar cell performance.

Recently, photoluminescence (PL) imaging has been demonstrated as a useful characterization technique that enables the measurement of the spatial distribution of the crystal defects related to carrier recombination.[5–7] In general, bright areas in the PL image indicate regions of higher minority carrier lifetime, whereas dark spots and lines show regions of lower minority carrier lifetime. However, it is difficult to distinguish whether the PL intensity reflects the intrinsic recombination activity of crystal defects or is influenced by decoration with impurities. Although a possible effect of defects in mc-Si on electrical properties has already been published elsewhere,[8,9] it still needs further experimental and theoretical support.

Our aim in this study is to determine and discuss the effects of crystal defects and their interactions with impurities on the electrical properties of mc-Si. We utilized samples grown by the floating cast method, and the growth was started by dendrite crystals at the top of the melt followed by solidification to the bottom. The resultant unique patterns of defects and impurities allowed us to elucidate the effects of different crystal defects and their interaction with impurities on the electrical properties of mc-Si.

II. EXPERIMENTS

A large mc-Si ingot was grown by the floating cast method using a silica crucible with an inner diameter of 23 cm. The inner wall of the crucible was coated with a silicon nitride (Si_3N_4) layer to prevent the cohesion between the ingot and the inner wall. A boron doped p-type Si feedstock of 10 kg was placed in the crucible and completely melted by heating it for about 10 h above 1490 °C in argon atmosphere in the furnace. The crystal growth was started with a faceted dendrite crystal on the upper surface of the melt, and the crystallization was directionally performed from the top to the bottom by a temperature drop at a cooling rate of 2 °C/h. The temperature distribution in the furnace was controlled to minimize the contact of the ingot with the crucible until the last stage of solidification.

After the growth experiments, a large mc-Si ingot was obtained and cut into a square block ($15.6 \times 15.6 \times 8\,cm^3$), as shown in Fig. 1(a). Since our attempt is to investigate the effects of impurities and their interactions with crystal defects on electrical properties, we focused on regions near the edge of the ingot to obtain samples with a high density of incorporated impurities. Therefore, a rectangular mc-Si rod with a cross-sectional area of about $1.7 \times 1.7\,cm^2$ was vertically cut out from the side edge region adjacent to the center block (Fig. 1(a)). From the selected rod, 400-μm-thick wafers were sliced perpendicularly to the grown direction (Fig. 1(b)), with a resistivity range of 1.1–1.3 Ω·cm. The wafers were numbered from 1, denoting the top of the ingot, to 57, denoting the bottom.

[a]Electronic mail: supawan.j@imr.tohoku.ac.jp

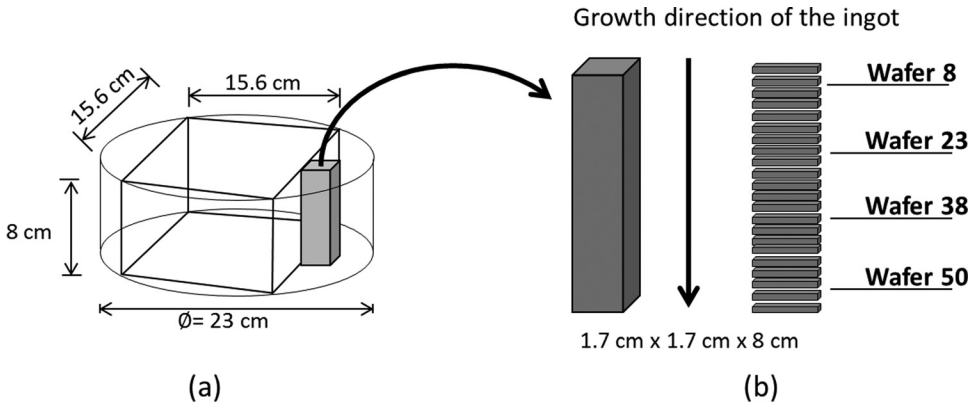

FIG. 1. (a) Multicrystalline Si block cut into 15.6×15.6 cm^2 from the grown ingot. (b) Schematic illustration of sample preparation for analysis.

As for the crystal growth mechanism, crystallization is ideally initiated from faceted dendrite crystals at the top of the melt, which leads to a small number of GBs by forming large grains. In addition, the external stress is assumed to be minimal at the initial stage, which results in a low density of dislocations in the top part of the ingot. In our experiment, wafer 1 was found to have a single GB, which was identified as a Σ27 boundary from the electron backscattering pattern (EBSP) measurement. Note that the very top of the ingot is contaminated with impurities from atmosphere.

During the ingot growth, GBs were generated from the Σ27 GB formed at the initial stage, and dislocation clusters developed around them. The number of dislocations increases downwards. At the final stage, the Si melt completely solidified and came in strong contact with the crucible wall. The impurity concentration should be very high at the bottom owing to the segregation from the molten phase and the solid state diffusion from the crucible wall.

On the basis of the growth mechanism, we have carefully selected four unique samples depending on the densities of impurities and dislocations from different ingot positions. Two samples with high impurities were first chosen from the top and bottom parts of the ingot, namely, a good area for the top part has no dislocations, while a poor one has a very high dislocation density covering most of the wafer surface. On the other hand, the other two samples with low impurities, the densities of which are assumed to be the same, were also selected from the central parts of the ingot. The selected samples are physically classified by impurity concentration and maximum local dislocation density in good (dislocation density $< 10^5$/cm^2) and poor (dislocation density $\geq 10^5$/cm^2) areas, as summarized in Table I. Dislocation density was determined using optical microscopy by counting etch pits and dividing the number obtained by the specific surface area.

TABLE I. Classification of mc-Si wafers prepared with different impurity concentrations and dislocation densities. Note that there are no good areas for the bottom wafer.

		Etch pit density, cm^{-2}	
Wafer position	Impurity level	Good area	Poor area
Top, 8th	High	no etch pits	2.9×10^5/cm^2
Moderate top, 23rd	Low	no etch pits	3.7×10^6/cm^2
Moderate bottom, 38th	Low	no etch pits	2.5×10^8/cm^2
Bottom, wafer 50th	High	1.5×10^6/cm^2	3.3×10^6/cm^2

The configuration of dislocations in the mc-Si wafers was directly determined by etch pit observation. Before the etch pit observation, the surface was mechanically polished on one side to achieve a nearly mirror-like smoothness and then chemically etched with Sopori etching solution[10] to obtain etch pits. For gettering impurities, the samples were annealed in an argon atmosphere at 835 °C for 10 s after coating with phosphorus oxide (P_2O_3) solution. Appropriate temperature and annealing time were chosen so that the impurities can sufficiently outdiffuse to the P_2O_3 layer. After annealing, the P_2O_3-contaminated diffusion layers were removed by chemical etching with HF and HNO_3 solution for 1 min.

Minority carrier lifetime was measured via microwave photoconductive decay (micro-PCD) to evaluate the recombination activity on mc-Si wafers before and after P diffusion. Lifetime maps on the wafers were obtained at a data spacing of 0.5 mm. PL images were taken using a Si charge-coupled device (CCD) camera (Hamamatsu C4742-98) using four light-emitting diodes (LEDs) with a wavelength of 532 nm and a total power density of about 10 mW/cm^2 as the excitation sources. An optical filter for near-infrared (NIR) light with a wavelength longer than 960 nm to pass through was placed at the entrance of the CCD camera. For the micro-PCD and PL imaging measurements, the sample surfaces were chemically passivated with quinhydrone methanol solution[11] for 1 h to obtain a very low surface recombination velocity. The surface recombination velocity prepared with this solution was reported to be 4.2 cm/s.[4] The total acquisition times for a single PL image and a micro-PCD lifetime map are 60 s and 30 min, respectively. We performed EBSP measurement to evaluate crystallographic orientation and GB characteristics. The obtained EBSP image was focused onto specific dislocation areas of selected samples with a scanning pitch of 5 μm and a maximum resolution of misorientation of about 2°.

III. RESULTS

Figure 2 shows the spatial distributions of minority carrier lifetime measured via micro-PCD of wafers 8, 23, 38, and 50 before and after P diffusion. It is seen that the average carrier lifetime in the mc-Si wafers increases with ingot height, then starts to decrease again at the very bottom of the ingot.

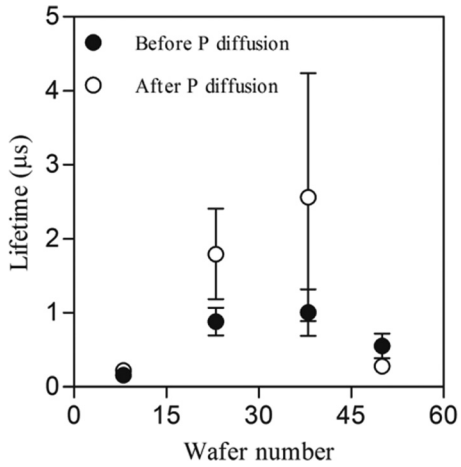

FIG. 2. Variation in minority carrier lifetime in mc-Si wafer from different positions before and after P diffusion.

At the top part of the ingot, the lifetime stays relatively low and external gettering is not efficient owing to the high level of hard-to-remove impurities coming from atmosphere, such as oxygen, carbon, and nitrogen.[12–14] Downwards to the central parts of the ingot, the initial lifetimes are rather high, and the gettering of impurities during P diffusion appears to become efficient (larger than 2 times). One possible reason is that heavy impurities were segregated downwards to the bottom part of the ingot during solidification, leaving a low density of impurities at the middle part of the ingot. At the very bottom part of the ingot, the lifetime decreased and external gettering was inefficient.

Figure 3 shows the distributions of minority carrier lifetime in the wafers before and after P diffusion. The difference between the background colors in lifetime mapping indicates the surface recombination rate. Blue and red regions show the highest and lowest lifetimes, respectively. Note that different scales have to be used for lifetime mapping comparison. The figures clearly reveal a distinctly inhomogeneous lifetime distribution. Upon P diffusion, there are significant changes, particularly in the defect-like regions (red regions), except for the top wafer. The impact of impurity interaction with crystal defects was also considered by

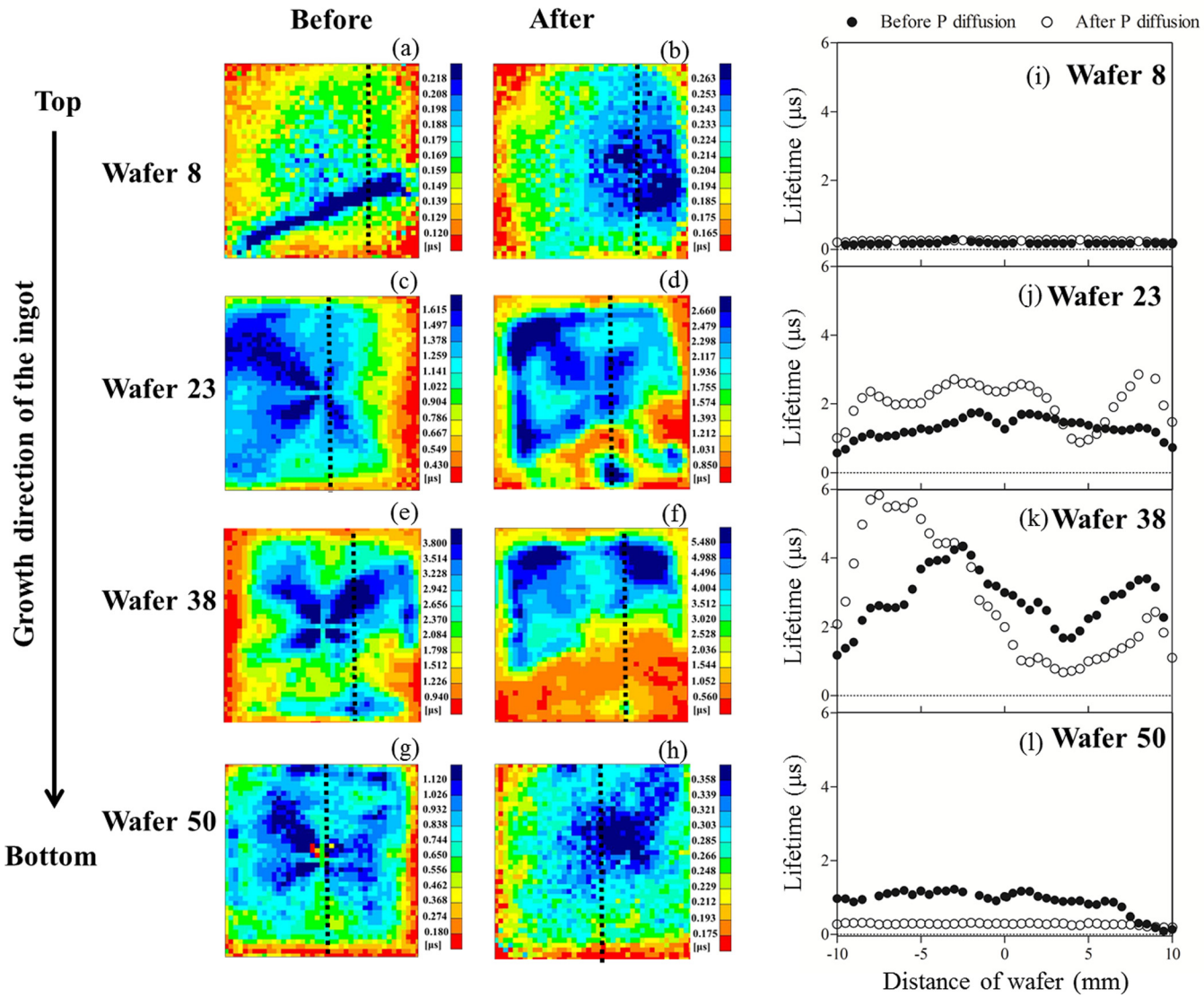

FIG. 3. (a)–(h) Distributions of minority carrier lifetime before and after gettering of impurities. (i)–(l) line scans of lifetimes across the wafers. Broken lines at the bottom of lifetime maps indicate the line scans across regions of a high defect density in Figs. 3(a)–3(h).

plotting line scans across defect like areas on the relative lifetime images (Figs. 3(a)–3(h)), as shown in Figs. 3(i)–3(l). By comparing wafers 23 and 38 (Figs. 3(j) and 3(k)), it is clear that the external gettering of impurities during P diffusion became efficient in regions of low defect density as evidenced by the increase in average minority lifetime. On the other hand, the decrease in the lifetime is significant in regions of higher defect density, which cannot be improved by P diffusion. Figure 4 shows a comparison of the PL images obtained before and after the gettering of impurities. Crystal defects such as GBs and dislocations can be identified in the PL map because of the difference in electrical activity. Electrically active GBs clearly appear as dark lines. In particular, if dislocations are clustered to form sub-GBs, the dark line patterns are significant. The comparison between Figs. 3 and 4 gives a spatially inhomogeneous lifetime reasonably correlated with the crystal grain structure and the dislocation density of different regions of the material.

As clearly seen from Figs. 2 and 3, the gettering of impurities by P diffusion becomes more efficient only for samples with a low density of impurities, as evidenced by the increase in minority carrier lifetime. In contrast, the decrease in the lifetime after P diffusion occurred in regions of high defect density. This result indicates that impurities precipitate at crystal defects, which limit the efficiency of the external gettering of impurities and reduce the lifetime.

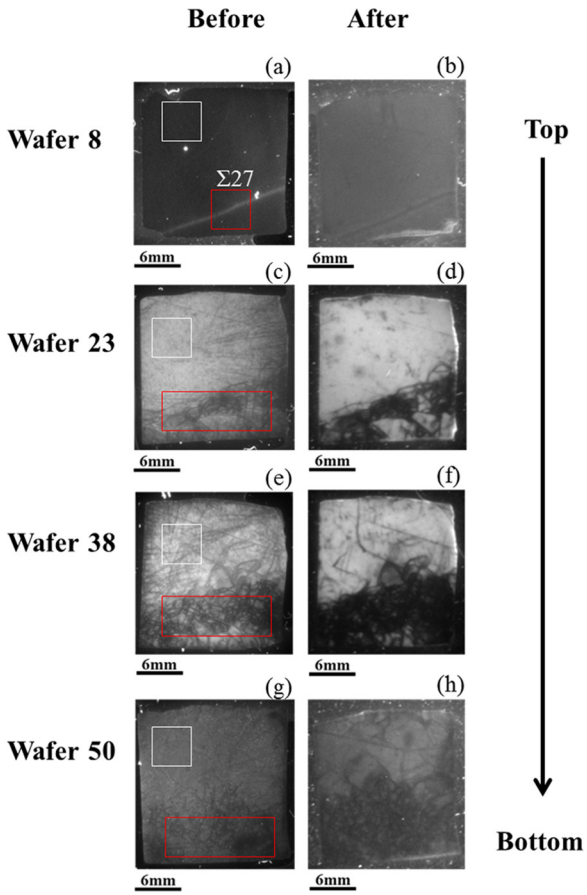

FIG. 4. Comparison of PL images taken before and after gettering of impurities. White squares indicate the good areas for the PL contrast plotted in Fig. 6, red squares indicate the poor areas (crystal defects) for the PL contrast plotted in Fig. 7.

From the results of the floating cast method, the top part of the sample consists of large crystal grains formed owing to the small nucleation rate, but has a high density of impurities from atmosphere. This leads to an anomalously bright Σ27 GB in the PL image (Fig. 4(a)) due to the internal gettering of impurities, leaving a clean area around the contaminated GB. The significant better cleaning was observed only at the GB after P diffusion (Fig. 4(b)), which is in agreement with our results of a slight improvement in minority carrier lifetime for the top wafer. During growth, the Σ27 GB can split into the Σ3 and Σ9 GBs with accompanying generation of dislocations and reduction in the density of impurities (Figs. 4(c) and 4(e)). Note that the scratches on the surface shown in Figs. 4(c) and 4(e) are due to the mechanical polishing process. After P diffusion (Figs. 4(d) and 4(f)), PL contrast was enhanced in regions of a high dislocation density (poor areas), whereas PL contrast in good areas revealed a small change compared with regions of a high dislocation density. This implies that impurities preferentially accumulate at GBs and dislocations that cannot be externally removed by P diffusion. At the final stage of the crystal growth, the sample contains high densities of segregated impurities and crystal defects originating from the strong contact with the crucible. A slight gettering of impurities (Figs. 4(g) and 4(h)) is observed, presumably due to the heavier impurities precipitated inside the defects.

IV. DISCUSSION

To explain the differences in electrical properties and the precipitation behavior of impurities between high-defect-density areas and no-crystal-defect areas, we use PL contrast defined by

$$PL_{contrast} = \frac{PL_b - PL_d}{PL_b}, \tag{1}$$

where PL_b and PL_d are the intensities in the bright and dark regions, respectively. Line profiles across good and poor areas were taken from the PL images indicated in the white squares in Fig. 4 before and after P diffusion. PL_d is the minimum intensity at defects and PL_b is the intensity in the flat region of the line profile. A decrease in PL contrast indicates that recombination at defects is suppressed, while an increase in PL contrast means that electrical activity is increased.[4]

Figure 5 shows the PL contrasts before and after P diffusion for good areas of all the samples with a dislocation density of less than $10^5/cm^2$. Our results demonstrate that there is no significant change in PL contrast for good areas of the samples with very low densities of impurities (wafers 23 and 38). This indicates that the incorporated impurities in these regions can be removed easily by gettering. For the wafers, we confirmed a positive effect of P diffusion; in addition, a high density of precipitated impurities was gettered and the minority carrier lifetime at good areas increased. In contrast, the sample of high dislocation density (wafer 50) became more active for recombination after P diffusion.

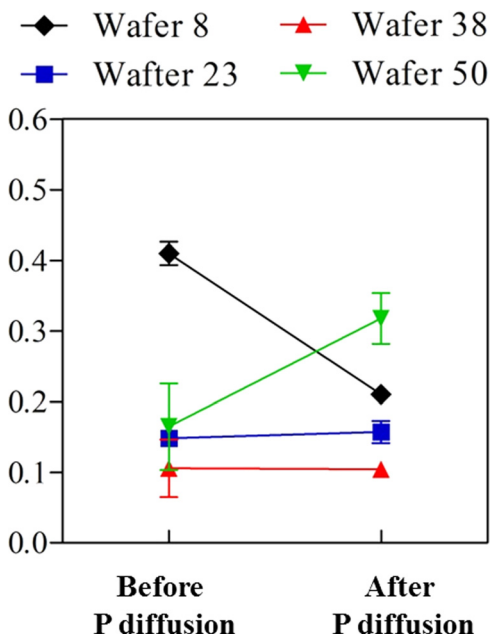

FIG. 5. PL contrasts before and after P diffusion for good areas (dislocation density $< 10^5/cm^2$), indicated by white squares in Fig. 4.

The local properties of crystal defects and their effects on electrical properties strongly depend on the type of crystal defect.[4,15,16] With respect to impurity precipitation at defects, we attempt to clarify the trends of preferential precipitation of impurities at certain types of boundary through their change after P diffusion. To this purpose, we attempted to determine the characteristics and type of GBs on wafer 23 by EBSP measurement. Figure 6 shows (a) an EBSP image, (b) a close-up inverse pole figure showing the orientation differences between individual crystals of specific area in Fig. 6(a) and 6(c) the distribution of etch pits in the region indicated by a broken-line square in Fig. 6(b). Most of the observed GBs were Σ3, Σ9, and Σ27, and no sub-GBs were observed because of the limitation of the angular resolution of the present EBSP measurement. We think that the blurry sub-GBs shown in the EBSP image, indicated by arrows in Fig. 6(b), were sub-GBs with a misorientation angle of less than 2° in the PL dark line pattern region. Additionally, we also confirmed the existence of sub-GBs by direct etch pit observation, as shown in Fig. 6(c).

To understand the interaction of impurities with different types of GB, line profiles were plotted across the individual coincidence site lattice (CSL), i.e., Σ3, Σ9, Σ27, and non-CSL (sub-GBs), as shown in the EBSP image. From the data (summarized in Fig. 7), GBs with a low CSL (or Σ) seem to contain lower densities of impurities than those with a high CSL or non-CSL. Generally, the precipitation of impurities is promoted with increasing Σ number, as evidenced by the increase in PL contrast (Figs. 7(a)–7(c)). For CSL boundaries, Σ27 GBs are the most recombination-active GBs and external gettering is inefficient for removing precipitated impurities. On the other hand, the accumulation of impurities was hardly observed at Σ9 GBs after P diffusion, and Σ3 GBs were found to be inactive, which are consistent with previous reports on the electrical activities of different types of GB.[17–19] These observations could be explained by the fact that a low-Σ boundary offers a lower density of energetically favorable sites for impurity atoms to segregate and precipitate, e.g., higher-Σ GBs will result in greater disorder around GBs.[20] For non-CSL, our results demonstrate that sub-GBs are the most recombination-active GBs, and external gettering is inefficient for removing impurities (Fig. 7(d)). Since GBs with very small angles of misorientation can be conceived as arrays of dislocations within crystals, these dislocations may act as preferred sites for the internal gettering of impurity atoms. This can be seen in Fig. 6(c) where sub-GBs are aligned perpendicular to the Σ9 GB.

To confirm the effect of dislocations on the precipitation behavior of impurities, the change in PL contrast after P diffusion across Σ27 GBs with/without dislocations is considered. Figure 7(c) shows that external gettering is inefficient for removing impurities only if Σ27 GB has dislocations. This result implies that there is a need to reduce the density of crystal defects to exploit impurity gettering by P diffusion

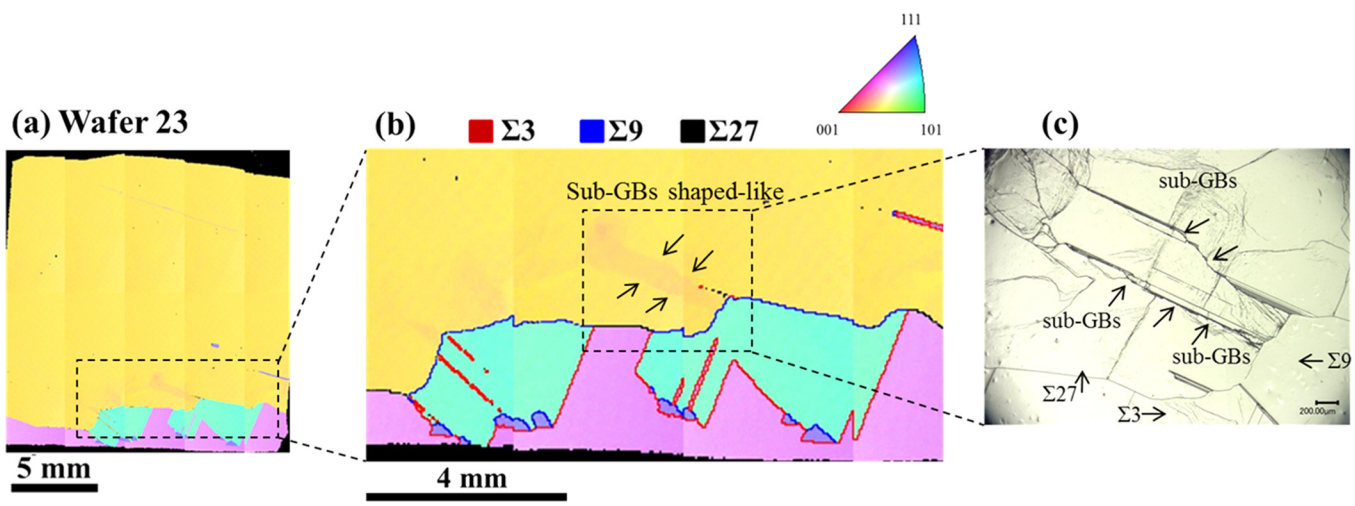

FIG. 6. (a) EBSP image of wafer 23. (b) Close-up EBSP image showing, crystallographic orientation image in region indicated by broken-line square in Fig. 6(a), (c) distribution of etch-pits on identical areas marked with broken square in Fig. 6(b). Arrows indicate sub-GBs.

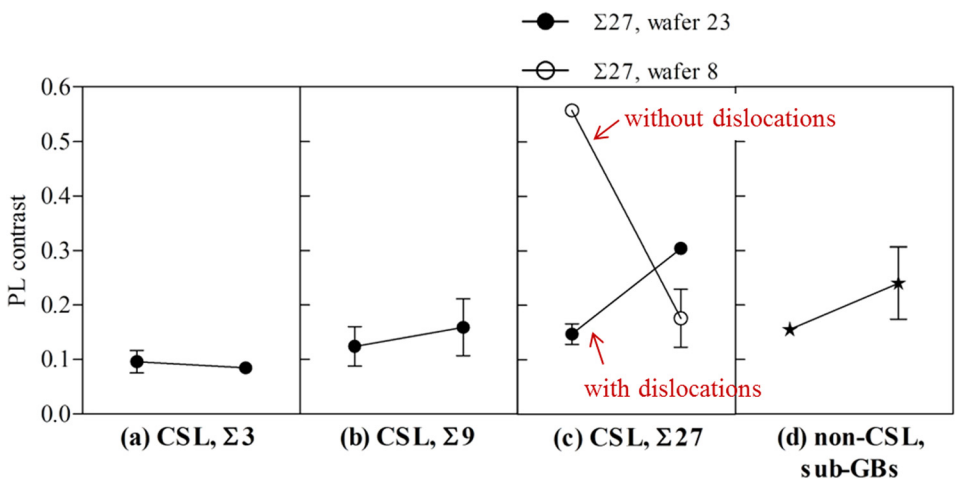

FIG. 7. PL contrasts before and after P diffusion for (a) CSL, Σ3, (b) CSL, Σ9, (c) CSL, Σ27, and (d) non CSL, sub-GBs.

in order to improve the electrical properties and yield of mc-Si for solar cells.

V. SUMMARY

We investigated the effects of different crystal defects and their interaction with impurities on the electrical properties of mc-Si using samples with unique defect patterns and impurities using the floating cast method. The top part of the sample consists of large crystal grains formed owing to the small nucleation rate, but has a high density of impurities from atmosphere. This leads to an anomalous bright Σ27 GB in the PL image because the degree of internal gettering of impurities at the GB becomes larger than that at the surrounding area, resulting in a cleaner area around the contaminated GB. However, external gettering is not efficient for improving the minority carrier lifetime owing to the high density of impurities. During crystal growth, the Σ27 GB can split into the Σ3 and Σ9 GBs with accompanying generation of dislocations and reduction in density of impurities. The external gettering of impurities during P diffusion then becomes efficient as evidenced by an increase in average minority carrier lifetime, while the PL contrast at certain types of defect increases owing to the accumulation of impurities. At the final stage of the crystal growth, the sample contains high densities of segregated impurities and crystal defects originating from the strong contact with the crucible. The decrease in such lifetime is significant, which cannot be improved by P diffusion. The increase in Σ is found to result in more enhanced precipitation of impurities, which leads to the poor gettering effect of P diffusion.

This confirms that the reduction in the densities of impurities and dislocations is crucial for improving the quality and yield of mc-Si ingots for solar cells. An attempt to improve the floating cast method is under way so that we can reduce the density of impurities from atmosphere as well as of dislocations by controlling inert gas flow and external stress.

ACKNOWLEDGMENTS

We thank Siliconplus Corporation for supplying the mc-Si ingot. This work was supported by the New Energy and Industrial Technology Development Organization (NEDO) of Japan.

[1]H. Sugimoto, K. Araki, and M. Tajima, J. Appl. Phys. **102**, 054506 (2007).
[2]S. He, S. Danyluk, I. Tarasov, and S. Ostapenko, Appl. Phys. Lett. **89**, 111909 (2006).
[3]G. Stokkan, S. Riepe, O. Lohne, and W. Warta, J. Appl. Phys. **101**, 053515 (2007).
[4]T. Kieliba, S. Riepe, and W. Warta, J. Appl. Phys. **100**, 063706 (2006).
[5]M. Tajima, Y. Iwata, F. Okayama, H. Toyota, H. Onodera, and T. Sekiguchi, J. Appl. Phys. **111**, 113523 (2012).
[6]T. Trupke, R. A. Bardos, M. C. Schubert, and W. Warta, Appl. Phys. Lett. **89**, 044107 (2006).
[7]H. Sugimoto, M. Inoe, M. Tajima, A. Ogura, and Y. Ohshita, Jpn. J. Appl. Phys. **45**, L641 (2006).
[8]D. Mankovics, R. P. Schmid, T. Arguirov, and M. Kittler, Cryst. Res. Technol. **47**, 1148 (2012).
[9]I. Takahashi, N. Usami, H. Mizuseki, Y. Kawazoe, G. Stokkan, and K. Nakajima, J. Appl. Phys. **109**, 033504 (2011).
[10]B. L. Sopori, J. Electrochem. Soc. **131**, 667 (1984).
[11]H. Takato, I. Sakata, and R. Shimokawa, Jpn. J. Appl. Phys., Part 2 **41**, L870 (2002).
[12]S. Martinuzzi, M. Gauthier, D. Barakel, I. Périchaud, N. Le Quang, O. Palais, and G. Goaer, Eur. Phys. J.: Appl. Phys. **40**, 83 (2007).
[13]S. Martinuzzi, I. Périchaud, and O. Palais, Sol. Energy Mater. Sol. Cells. **91**, 1172 (2007).
[14]D. Macdonald, A. Cuevas, A. Kinomura, and Y. Nakano, in *Conference Record of the 29th IEEE Photovoltaic Specialists Conference, New Orleans, LA, 2002* (IEEE Cat. No. 02CH37261), p. 285.
[15]K. Kutsukake, N. Usami, T. Ohtaniuchi, K. Fujiwara, and K. Nakajima, J. Appl. Phys. **105**, 044909 (2009).
[16]J. Chen and T. Sekiguchi, Jpn. J. Appl. Phys., Part 1 **46**, 6489 (2007).
[17]J. Lu, M. Wangener, G. Rozgonyi, J. Rand, and R. Jonczyk, J Appl. Phys. **94**, 140 (2003).
[18]J. Chen, T. Sekiguchi, D. Yang, F. Yin, K. Kido, and S. Tsurekawa, J. Appl. Phys. **96**, 5490 (2004).
[19]J. Chen, D. Yang, X. Zhenqiang, and T. Sekiguchi, J. Appl. Phys. **97**, 033701 (2005).
[20]M. D. Pickett, A. A. Istratov, E. Sauar, T. C. Lommasson, E. Marstein, T. Pernau, R. F. Clark, S. Narayanan, S. M. Heald, and E. R. Weber, *Conference Record of the 4th IEEE Photovoltaic Energy Conference, Waikoloa, Hawaii* (2006), p. 944.